Interpretable machine learning for prediction and inverse design of electrical resistivity multicomponent aluminium alloys

Deni Haryadi
Department of Mechanical Engineering, Gunadarma University, Depok 16424, Indonesia

Aji Abdillah Kharisma
Department of Mechanical Engineering, Gunadarma University, Depok 16424, Indonesia

Hamzah Ali Nashirudin
Department of Mechanical Engineering, Politeknik Purbaya, Tegal 52193, Indonesia

Haris Rudianto
Department of Mechanical Engineering, Gunadarma University, Depok 16424, Indonesia

Abstract: Aluminium is the standard interconnect metal in CMOS technology and can be deposited at low temperature, yet its intrinsically low electrical resistivity makes it inefficient as a Joule heating element, forcing microheater designs toward platinum or polysilicon at the cost of process complexity. This study reframes the problem as one of composition engineering rather than material substitution and develops a machine learning framework to predict and inversely design the electrical resistivity of aluminium alloys. A curated dataset of 220 commercial alloys, described by nine compositional features (Si, Fe, Cu, Mn, Mg, Cr, Zn, Ti, Zr) and spanning 2.80–6.40 μΩ·cm, was assembled from a public materials database. Four regression models were benchmarked: Linear Regression (R^2 = 0.635), Support Vector Regression (R^2 = 0.821), Random Forest (R^2 = 0.837), and Extreme Gradient Boosting, which performed best on an independent hold-out test partition (test R^2 = 0.861; test MAPE = 3.9%) and remained stable under k-fold cross-validation carried out within the training partition (CV-R^2 = 0.839; CV-RMSE = 0.396 μΩ·cm). The pronounced gap between the linear baseline and the non-linear learners confirms that resistivity in multicomponent aluminium alloys is governed by interacting solute effects. Feature importance analysis identified magnesium (0.554), copper (0.215), and zinc (0.153) as the dominant contributors, accounting for approximately 92% of the model's explanatory power, consistent with solid-solution and

Correspondents Author:
Deni Haryadi, Department of Mechanical Engineering, Gunadarma University, Depok 16424, Indonesia
Email: deniharyadi@staff.gunadarma.ac.id

Received April 26 2026; Revised July 21, 2026; Accepted July 21 2026; Published July 22, 2026

impurity scattering mechanisms. Surrogate-based inverse screening produced heavily alloyed Al–Zn–Mg–Cu candidates with predicted resistivity of 9.26–9.52 μΩ·cm. These values lie outside the multivariate domain of the training data: the candidates carry 24.2–32.3 wt.% total solute, leaving an aluminium balance of only 67.7–75.8 wt.%, and they exceed the training maximum for Cu, Zn and Zr in every case. They are therefore reported as an extrapolative indication of direction in composition space rather than as validated alloy candidates, and require aluminium-balance constraints, thermodynamic screening and experimental validation before any device-level claim can be made.

Keywords: aluminium alloys, electrical resistivity, machine learning, inverse alloy design.

Introduction

Rapid progress in microsystems and smart sensing technologies has intensified the demand for miniaturized thermal components capable of fast, stable, and energy-efficient heat generation. In applications such as gas sensing, polymerase chain reaction (PCR) and DNA thermal cycling, and thermally triggered drug delivery, precise temperature control directly determines device sensitivity, selectivity, and reliability. At the heart of these systems are microheaters, whose performance is fundamentally governed by Joule heating efficiency, which in turn depends on both the intrinsic electrical resistivity of the heater material and the geometric design of the heating element. As device dimensions continue to shrink and integration density increases, the choice of heater material becomes increasingly critical for balancing thermal performance, power consumption, and manufacturability. State-of-the-art MEMS microheaters predominantly rely on platinum, polysilicon, and selected metal alloys. Platinum is widely adopted due to its excellent electrical conductivity, thermal stability at elevated temperatures, and minimal drift during long-term operation, making it suitable for high-performance microheaters requiring stable temperature output (Kalinin et al., 2023). Polysilicon microheaters, although exhibiting lower thermal conductivity than metals, are attractive because they can be readily fabricated using standard semiconductor processes, allowing seamless integration with other microfabricated components in lab-on-a-chip and sensing platforms (Krishna et al., 2022). More recently, tailored metal alloys have been explored to improve resistance to thermal cycling and mechanical degradation, with aluminum-based alloys containing magnesium or zinc demonstrating improved mechanical robustness under repeated heating–cooling cycles (Abdo et al., 2021). Beyond material selection, microheater architectures also play a decisive role in thermal performance. Serpentine trace designs are commonly employed to increase effective resistance and promote uniform temperature distribution across the active area, thereby improving heating efficiency

and reducing thermal gradients (Li et al., 2022). Emerging three-dimensional architectures further enhance thermal efficiency by improving coupling between heaters and sensing elements, particularly in gas sensor platforms where rapid thermal response is essential (Jeroish et al., 2022). Performance evaluation of MEMS microheaters typically focuses on operating temperature, heating ramp rate, thermal stability, and power consumption. Recent reports indicate heating ramp rates exceeding 100 °C s^{-1}, which are critical for reducing response times in sensing and PCR applications (Jeroish et al., 2022). At the same time, power consumption below 100 mW has become a key target for portable and battery-powered systems, underscoring the importance of energy-efficient heater design (Li et al., 2022).

A central factor underlying these performance metrics is the electrical resistivity of the heater material. According to Joule's law, the generated thermal power is proportional to the square of the applied current and the electrical resistance of the heater ($P = I^2R$). Consequently, materials with higher resistivity can generate sufficient heat at lower currents, reducing electrical stress on driver circuits and improving overall energy efficiency (Jeroish et al., 2022). Conversely, materials with very low resistivity require higher operating currents to reach target temperatures, which can increase power consumption and exacerbate reliability issues. Electrical resistivity also affects temperature uniformity and hotspot formation, which are critical for consistent operation at the microscale (Li et al., 2022).

Reliability considerations further complicate material selection for thin film microheaters. Common failure mechanisms include electromigration, oxidation, thermal fatigue, and delamination, all of which are closely linked to material properties and operational conditions. Electromigration, driven by high current densities, is particularly problematic in highly conductive metals such as aluminum and copper, where atomic migration can lead to void formation and eventual circuit failure (Kalinin et al., 2023). Oxidation poses an additional risk for aluminum-based heaters, as oxide layer formation can alter resistivity and accelerate degradation under repeated heating cycles (Kalinin et al., 2023). Thermal fatigue arising from cyclic expansion and contraction can induce cracking in thin films, while delamination may occur due to thermal expansion mismatch between metallic layers and silicon-based substrates (Li et al., 2022; Kalinin et al., 2023). Collectively, these issues highlight the need for materials that not only provide suitable resistive heating but also maintain structural and electrical integrity during prolonged operation. From a manufacturing perspective, CMOS compatibility is a decisive requirement for large-scale integration of microheaters with electronic circuitry. Platinum and polysilicon, although reliable, often require higher deposition or processing temperatures, typically exceeding 300 °C, which can limit compatibility with low-temperature CMOS back-end processes (Krishna et al., 2022). Aluminum, in contrast, is a standard interconnect material in CMOS technology and can be

deposited at relatively low temperatures around 150–200 °C, offering significant advantages in terms of cost, scalability, and integration simplicity (Jeroish et al., 2022). Aluminum-based microheaters can be fabricated using established sputtering or evaporation techniques followed by conventional photolithography, enabling straightforward co-integration with sensors and readout electronics (Jeroish et al., 2022). However, these advantages are offset by aluminum's intrinsically low electrical resistivity, which renders it excessively conductive for efficient resistive heating at the microscale. The low resistivity of pure aluminum necessitates high operating currents to achieve target temperatures, leading to increased power consumption and heightened susceptibility to electromigration and thermal fatigue. Several studies have demonstrated aluminum thin-film microheaters in MEMS platforms but consistently report challenges associated with poor thermal efficiency and long-term reliability due to high conductivity (Jeroish et al., 2022; Kalinin et al., 2023). As device dimensions shrink further, these limitations become more pronounced, motivating the need for strategies that can increase aluminum's resistivity while preserving its CMOS compatibility and low-cost processing advantages. Materials science offers several pathways to modify the electrical resistivity of aluminum. Alloying with elements such as copper, magnesium, silver, zinc, or selected transition metals can increase resistivity through solid-solution scattering and impurity effects, while simultaneously enhancing mechanical strength (Abdo et al., 2021; Alshwawreh et al., 2021; Cui et al., 2023; Yavari et al., 2025). Microstructural control, including grain refinement via severe plastic deformation or tailored heat treatments, has also been shown to increase resistivity by enhancing grain boundary scattering (Genc et al., 2022; Liu et al., 2025). Controlled aging and annealing processes further influence solute distribution and precipitation behavior, providing additional levers to tune electrical properties (Bai et al., 2025; Khan & Sasikumar, 2025). Nevertheless, these approaches must remain compatible with MEMS fabrication constraints, including thermal stability, processability, and thin-film deposition requirements. Despite these advances, systematic design of aluminum alloys specifically optimized for resistive heating applications remains limited. Most existing studies explore isolated alloy systems or processing routes without a comprehensive framework to navigate the high-dimensional composition space efficiently. Given the non-linear and interacting effects of multiple alloying elements on electrical resistivity, traditional trial-and-error experimentation becomes increasingly inefficient. In this context, data-driven approaches based on machine learning offer a powerful alternative by learning complex composition–property relationships directly from existing data and enabling rapid screening of candidate materials.

This study therefore advances an artificial intelligence–driven framework for the design of high-resistivity aluminum alloys tailored for energy-efficient heating element applications. By

treating electrical resistivity as the primary performance parameter linking alloy composition to Joule heating efficiency, the alloy design problem is reframed as a data-driven optimization task rather than a purely empirical metallurgical exercise. Machine learning models are employed to capture non-linear relationships between alloying elements and resistivity, and to guide inverse design toward compositions that maximize resistivity while remaining realistic for CMOS-compatible fabrication. The central contribution of this work lies in demonstrating that aluminum intrinsic limitations as a microheater material can be overcome through composition engineering guided by machine learning. By shifting the focus from material substitution to property optimization within a CMOS-compatible material system, this approach provides a scalable pathway toward low-cost, integrable, and energy-efficient microheaters for sensing and biomedical technologies. In doing so, the study bridges materials science, microfabrication, and data-driven design, offering a generalizable framework for tailoring functional properties of engineering alloys for microscale applications.

Relative to existing machine learning studies on aluminium alloys, the contribution of this work is distinguished in three respects. First, the design objective is inverted. Prior data-driven studies on aluminium have almost uniformly sought to maximise electrical conductivity while retaining mechanical strength, for conductor, busbar and wire applications (Liang et al., 2022; Genc et al., 2022; Yavari et al., 2025); the present work treats resistivity as the quantity to be maximised for Joule-heating efficiency, which relocates the optimum to a region of composition space that conductor-oriented studies deliberately avoid, and which is therefore poorly represented in the existing modelling literature. Second, previous interpretable machine learning frameworks for alloy design have targeted structural or mechanical properties, principally in TiAl and titanium aluminide systems (Kwak et al., 2022; Padhy et al., 2025). Here the property model is coupled to a device-level requirement, namely CMOS-compatible thin-film microheater operation, so that model output is interpreted against a specific fabrication constraint rather than against a generic property target. Third, the forward model is not reported in isolation: it is used as a surrogate for inverse screening whose degree of extrapolation is quantified explicitly against the training domain, and whose unconstrained output is reported as a directional indication rather than as a set of recommended compositions. To the best of the authors' knowledge, no previous study has framed aluminium alloy design around resistivity maximisation for integrated microheaters, nor reported the applicability-domain analysis that such an inverted objective necessarily requires.

Research Method

Data Collection and Database Construction

The dataset used in this study was constructed to support data-driven prediction and inverse design of electrical resistivity in aluminum alloys. Raw data were collected from the MatWeb materials (https://www.matweb.com) property database, which is widely recognized as a standardized repository for engineering alloy compositions and measured physical properties. An initial data harvesting step yielded approximately 439 raw entries spanning a wide range of commercial aluminum alloy series and electrical resistivity values were collected at T = 20 °C. This broad coverage was intentionally targeted to ensure sufficient compositional diversity and to reduce model bias toward any single alloy family. Given the heterogeneous nature of public materials databases, a rigorous data curation protocol was implemented prior to model development. Duplicate records were identified and removed using automated filtering routines based on matching alloy composition ranges, alloy designations, and reported resistivity values. To minimize the risk of inadvertently removing physically meaningful variations, automated screening was complemented by rule-based checks to ensure that records with distinct compositions or measurement contexts were retained, in line with best practices for materials database construction (Liang et al., 2022). Entries containing missing or incomplete resistivity values were excluded from the target dataset. For compositional fields, records with partially missing elemental weight fractions were also removed rather than imputed, as resistivity prediction in multicomponent alloys is highly sensitive to solute content. This conservative filtering strategy prioritized data reliability over dataset size, following recommendations for materials informatics studies where noise can significantly degrade model performance (Kwak et al., 2022). Outliers in resistivity were evaluated using statistical thresholds based on interquartile range analysis. Extreme values were inspected in context and removed only when clearly inconsistent with reported alloy compositions or measurement norms, consistent with contextual outlier handling approaches proposed in recent literature (Elamin et al., 2025). After completing the data cleaning and validation procedures, the final curated dataset comprised 220 aluminum alloy data points, each containing a complete set of compositional descriptors and a corresponding electrical resistivity value. For transparency, the curation outcome is reported quantitatively. Of the 439 harvested records, 219 for missing or incomplete resistivity values, leaving the 220 records used for modelling. Outliers were flagged using the 1.5 × interquartile range criterion applied to the resistivity distribution and were removed only after inspection against the reported composition, so that physically plausible extremes were retained. Where the source database specifies an alloying element as a permitted concentration range rather than a single value,

the midpoint of the range was taken as the feature value; elements not listed for a given alloy were encoded as 0 wt.%. This convention introduces a known source of label noise, since the actual composition of any given heat may lie anywhere within the specified range, and it places a floor on the residual error that no choice of algorithm can remove. The alloy designations of all 220 retained records are listed in Supplementary Table S1.

Feature Definition and Statistical Description

The machine learning models developed in this work rely exclusively on alloy composition as the input feature space. Processing history and microstructural metadata were not included, as such information is inconsistently reported across public databases and would substantially reduce usable data volume. This composition-only approach is consistent with prior resistivity and conductivity prediction studies in aluminum and other alloy systems. Nine alloying elements were selected as predictive features based on their prevalence in commercial aluminum alloys and their known influence on electrical properties: silicon (Si), iron (Fe), copper (Cu), manganese (Mn), magnesium (Mg), chromium (Cr), zinc (Zn), titanium (Ti), and zirconium (Zr). Each feature was expressed as weight percentage (wt.%). The target variable was electrical resistivity, reported in micro-ohm centimeter (μΩ·cm).

Table 1 Statistical Summary of the Aluminum Alloy Dataset

Type	Parameter	Minimum	Maximum	Mean
Inputs	Si (wt.%)	0.0400	12.2500	0.5656
	Fe (wt.%)	0.0500	1.0000	0.2983
	Cu (wt.%)	0.0000	6.3000	0.9690
	Mn (wt.%)	0.0000	1.2500	0.2869
	Mg (wt.%)	0.0000	5.1000	1.6438
	Cr (wt.%)	0.0000	0.2500	0.0917
	Zn (wt.%)	0.0200	7.8000	0.9737
	Ti (wt.%)	0.0000	0.2000	0.0574
	Zr (wt.%)	0.0000	0.1750	0.0131
Outputs	Resistivity (μΩ·cm)	2.8000	6.4000	4.3660

The wide compositional and resistivity ranges summarized in Table 1 provide a suitable foundation for training non-linear machine learning models capable of learning complex composition–property relationships.

Machine Learning Model Development

Four supervised regression algorithms were implemented and compared to predict aluminum alloy resistivity: Linear Regression, Support Vector Regression (SVR), Random Forest, and Extreme Gradient Boosting (XGBoost). All models were implemented using the Python programming language, primarily leveraging the Scikit-learn ecosystem, with XGBoost implemented via its dedicated library. Linear Regression was employed as a baseline model to assess the extent to which resistivity could be approximated as a linear combination of alloying elements. While computationally efficient and interpretable, linear regression is known to perform poorly when strong non-linear interactions dominate the underlying physical behavior (Kwak et al., 2022). Support Vector Regression with a radial basis function (RBF) kernel was selected to model non-linear dependencies between composition and resistivity. The RBF kernel enables projection of the input space into higher-dimensional feature spaces, allowing the model to fit complex response surfaces. Key hyperparameters, including the penalty factor (C), kernel width (γ), and error tolerance (ε), were tuned to balance model complexity and generalization (Liang et al., 2022).

Random Forest regression was applied as an ensemble learning approach that aggregates predictions from multiple decision trees constructed using bootstrap sampling. This method is particularly effective for materials datasets with mixed feature importance and non-linear interactions, as it reduces variance and mitigates overfitting through averaging (Kwak et al., 2022). XGBoost was selected as a state-of-the-art gradient boosting method that constructs decision trees sequentially to minimize residual errors. Its regularized objective function and built-in handling of missing values make it well suited for sparse or noisy materials datasets. Despite requiring careful hyperparameter tuning, XGBoost has demonstrated superior accuracy and scalability in alloy property prediction tasks (Padhy et al., 2025).

Model Training and Evaluation Protocol

To ensure robust performance assessment, the 220 records were divided into a training partition and an independent hold-out test partition in a 80:20 ratio using a fixed random seed so that the split is exactly reproducible. Every hold-out metric reported below was computed exclusively on the test partition, which was never used for model selection or hyperparameter tuning. Model generalisation was additionally assessed by k-fold cross-validation (k = shuffled, same seed) carried out within the training partition only. Because Support Vector Regression and Linear Regression are sensitive to feature scale, the input features were standardised to zero mean and unit variance, with the scaler fitted on the training folds alone and then applied to the validation and test data, so that no information from held-out data entered the fitting process. Random Forest and XGBoost are invariant to

monotonic feature scaling and were trained on the raw weight-percentage features. In this approach, the dataset was partitioned into k equally sized folds; each fold was used once as a validation set while the remaining k−1 folds were used for training. This procedure reduces sensitivity to a single train–test split and provides a more reliable estimate of predictive performance (Kwak et al., 2022). Model accuracy was quantified using three complementary error metrics. The coefficient of determination (R^2) was used to evaluate goodness of fit and the proportion of variance in resistivity explained by the model (Liang et al., 2022). The root means square error (RMSE) provided an absolute measure of prediction error in units of μΩ·cm, which is particularly relevant for resistivity optimization tasks (Padhy et al., 2025). Mean absolute percentage error (MAPE) was used to express prediction error in relative terms, facilitating comparison across models with different error distributions (Elamin et al., 2025).

Inverse Design Framework

Hyperparameter Optimisation

Hyperparameters for Support Vector Regression, Random Forest and XGBoost were tuned by rid search over the search ranges listed in Supplementary Table S2, using k-fold cross-validation applied to the training partition only. For each candidate configuration, the mean cross-validated R^2 across folds served as the selection criterion; the best configuration was then refitted on the full training partition and evaluated once against the hold-out test partition. Linear Regression has no tunable hyperparameters and was fitted directly. The selected values for each model are given in Supplementary Table S2 alongside the search ranges. It should be stated plainly that this protocol is a single-loop rather than a nested cross-validation: model selection and the cross-validated statistics reported below draw on the same folds, so those statistics carry a mild optimistic bias. The hold-out test partition was excluded from the tuning loop entirely and is free of this bias, which is why hold-out and cross-validated metrics are reported separately throughout rather than being pooled. Nested cross-validation, in which an outer loop provides the performance estimate while an inner loop performs selection, would remove the residual bias and is identified among the limitations as a refinement for subsequent work; with 220 records it was not adopted here because the inner training folds would fall below the size at which the tree ensembles train stably. Following validation of forward prediction accuracy, the best-performing model was employed as a surrogate for inverse alloy design. In this framework, hypothetical aluminium alloy compositions were generated by sampling over per-element intervals running from the training minimum to ⟨1.2⟩ × the training maximum for each of the nine compositional features, that is, within and moderately beyond the univariate compositional bounds of the

training dataset. The trained model was then used to predict resistivity for each candidate composition, enabling rapid screening of large regions of composition space. Candidate alloys were ranked according to predicted resistivity, and top-performing compositions were selected as potential high-resistivity aluminum alloys suitable for microheater applications. While no explicit thermodynamic or phase-stability constraints were imposed at this stage, the inverse design results were interpreted as guidance for subsequent experimental validation rather than definitive material solutions. Two constraints that a deployable inverse-design pipeline would impose were deliberately not enforced at this stage, and this is stated in advance because it bounds the interpretation of everything that follows. First, no aluminium-balance constraint was applied, so the sampler was free to raise several solutes towards their individual upper bounds simultaneously; because the bounds are applied element by element, a composition can satisfy every univariate constraint while carrying a total solute content far outside anything present in the training data. Second, no thermodynamic screening for phase stability, equilibrium solid solubility or solidification behaviour was performed, so compositions that could not be produced as single-phase or near-single-phase material were not excluded. The consequences of both omissions are quantified in the applicability-domain analysis below, and a constrained formulation that reverses the ordering, applying the physical screens before rather than after prediction, is set out in the Discussion.

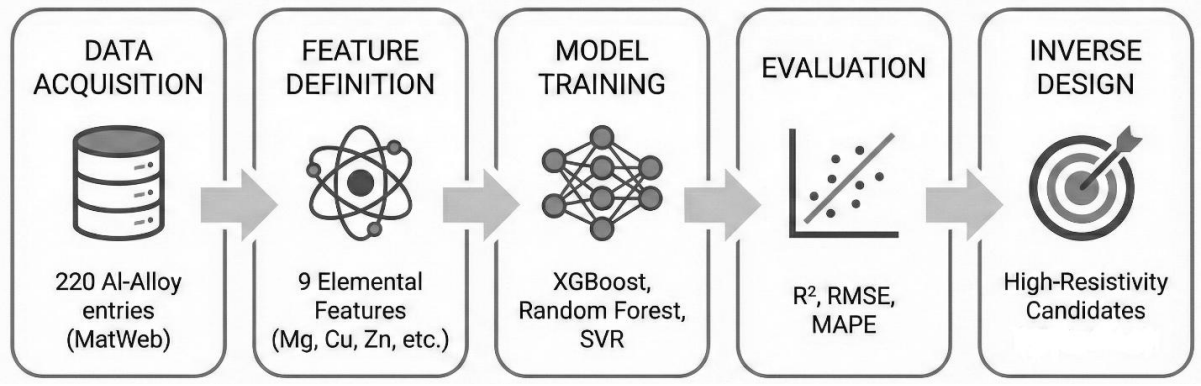

Figure 1 Schematic workflow of the data-driven methodology, illustrating database construction, feature definition, machine learning model training, evaluation, and inverse alloy design.

Result and Discussion

Results

Predictive performance of machine learning models

The predictive capability of four regression models Linear Regression, Support Vector Regression (SVR) with a radial basis function kernel, Random Forest, and Extreme Gradient Boosting (XGBoost) was assessed by comparing predicted electrical resistivity values against experimental reference values. Figure 2 summarizes the parity plots for all models on the held-

out test set, together with the associated coefficient of determination (R^2) and mean absolute percentage error (MAPE). The linear baseline provided the weakest performance (R^2 = 0.635; MAPE = 8.1%), indicating that a purely additive model is insufficient for capturing the resistivity response surface in multicomponent aluminum alloys. In contrast, SVR substantially improved predictive accuracy (R^2 = 0.821; MAPE = 5.5%), consistent with its capacity to represent non-linear mappings in composition-only datasets.

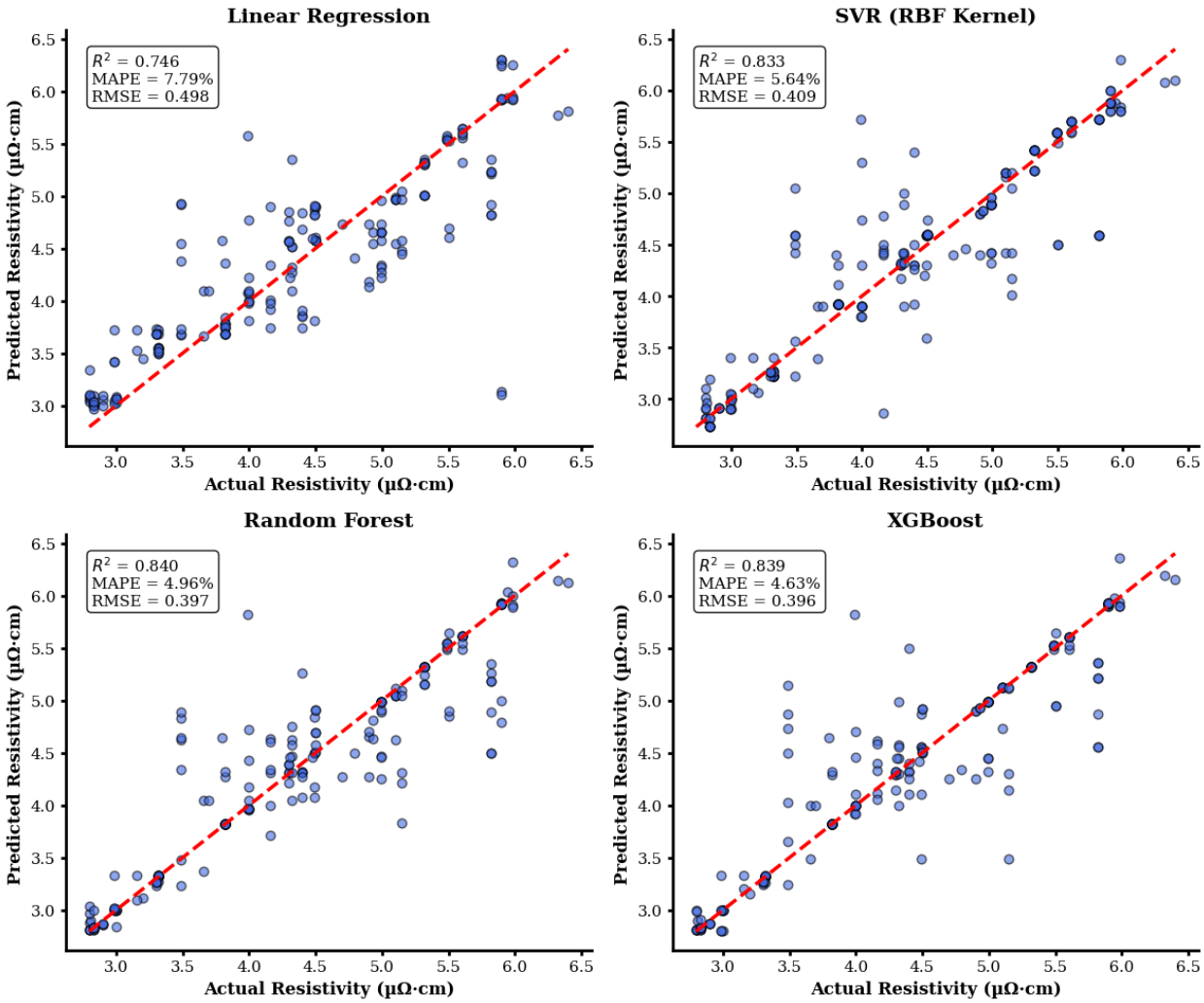

Figure 2 Predicted versus experimental electrical resistivity for (a) Linear Regression, (b) SVR (RBF), (c) Random Forest, and (d) XGBoost on the test set.

Tree-based ensemble learners offered the strongest overall performance. Random Forest yielded R^2 = 0.837 and MAPE = 4.6%, while XGBoost achieved the highest accuracy with R^2 = 0.861 and MAPE = 3.9%. The tighter clustering of predictions around the 1:1 line in Figure 2d indicates that gradient boosting reduced systematic bias and minimized large deviations across the resistivity range. These results align with prior benchmarking studies in alloy property prediction, where Linear Regression commonly attains modest R^2 values, while SVR improves performance and ensemble methods (Random Forest and XGBoost) frequently

achieve the highest accuracy due to their ability to capture feature interactions and complex non-linearities (Liang et al., 2022; Kwak et al., 2022). The observed MAPE values also fall within literature-reported ranges for resistivity prediction, with the best ensemble model approaching the lower bound typically reported for well-curated datasets (Padhy et al., 2025; Elamin et al., 2025). The marked performance gap between Linear Regression and the non-linear models provides quantitative evidence that resistivity in multicomponent aluminum alloys is governed by non-linear composition–property relationships. Such non-linearity is expected because multiple alloying elements jointly modulate electron scattering through solid-solution distortions, impurity scattering, and microstructural pathways associated with precipitation and intermetallic formation. These coupled mechanisms create interaction effects that cannot be adequately represented by linear superposition (Abdo et al., 2021; Cui et al., 2023). The comparative results in Figure 2 support this interpretation. Linear Regression exhibits broader dispersion and larger residuals, particularly away from the mid-range, whereas SVR and the ensemble models reduce dispersion by learning non-linear decision boundaries in the composition space. This behavior is consistent with prior reports that ensemble methods and other non-linear learners (including neural networks and Gaussian processes) outperform linear baselines for property prediction in compositionally diverse alloy datasets (Liang et al., 2022; Kwak et al., 2022).

Cross-validation performance and robustness

To evaluate robustness and reduce sensitivity to a single train–test split, K-fold cross-validation was performed for all models. K-fold cross-validation was performed within the training partition for all models. Table 2 summarises the cross-validated R^2, RMSE and MAPE values. These are cross-validated statistics and are not interchangeable with the hold-out test metrics quoted in the preceding subsection; the two families of metric are computed on different data under different protocols and are reported separately throughout this manuscript to prevent conflation. Where a single figure of merit is required for the best model, the hold-out test values (R^2 = 0.861; MAPE = 3.9%) are the appropriate ones to quote, since they alone derive from data untouched by model selection. Random Forest and XGBoost maintained the highest and most stable predictive performance (CV-R^2 ≈ 0.84), with low absolute error (CV-RMSE ≈ 0.396–0.397 μΩ·cm) and modest relative error (CV-MAPE ≈ 4.63–4.96%). SVR followed closely (CV-R^2 = 0.8326), while Linear Regression remained substantially lower (CV-R^2 = 0.7463), reinforcing that non-linear models provide the most reliable generalization for this dataset. These results are consistent with recommended reporting practices in materials machine learning, where cross-validated mean performance is used to complement holdout test metrics and to highlight stability across folds (Kwak et al., 2022; Elamin et al., 2025). Prior studies further indicate that the choice of k (commonly 5–

10), shuffling, and stratification by alloy family can materially affect stability and fairness of performance estimates; therefore, cross-validation metrics should be interpreted in conjunction with test-set results to identify potential overfitting (Kwak et al., 2022; Padhy et al., 2025).

Table 2 K-fold cross-validation results for all models.

Algorithm	R^2 Score	RMSE (μΩ·cm)	MAPE (%)
Random Forest	0.8402	0.3973	4.9596
XGBoost	0.8392	0.3960	4.6317
SVR (RBF Kernel)	0.8326	0.4090	5.6447
Linear Regression	0.7463	0.4981	7.7929

Feature importance and interpretability of the XGBoost model

Beyond predictive performance, an interpretable understanding of the composition–resistivity drivers is essential for actionable alloy design. Feature importance analysis was therefore conducted using the trained XGBoost model. As shown in Figure 3, magnesium (Mg) was the dominant factor influencing electrical resistivity, with a relative importance of 0.5538, indicating that variation in Mg accounts for more than 55% of the model's explanatory power. Copper (Cu) and zinc (Zn) followed with importance scores of 0.2148 and 0.1532, respectively, and together Mg–Cu–Zn contributed approximately 92% of the total importance.

This ranking is metallurgically plausible and aligns with established scattering mechanisms in aluminum alloys. Increasing Mg content enhances solid-solution electron scattering through lattice distortion, while Cu and Zn additions introduce additional scattering centers and can promote precipitate or intermetallic formation pathways that further modify electron transport (Abdo et al., 2021; Cui et al., 2023; Khan & Sasikumar, 2025; Yavari et al., 2025). Lower-ranked variables (Fe, Cr, Zr) contributed negligibly in this dataset, suggesting that within the observed concentration ranges their influence on resistivity is either intrinsically weaker or masked by the stronger effects of the major solutes. From a materials informatics standpoint, this type of global attribution is commonly derived from gain-based importance in tree models, while permutation importance and SHAP can provide complementary, more interaction-aware explanations (Liang et al., 2022; Padhy et al., 2025). While the present analysis uses model-intrinsic importance, future work could incorporate SHAP to strengthen interpretability at both global and local (composition-specific) scales.

Two caveats attach to this ranking and are stated here rather than deferred. Gain-based importance in gradient-boosted trees is computed from the reduction in the training objective at each split, and it is known to be biased towards features offering many distinct split points and to allocate the shared contribution of correlated features to whichever of them is selected first. Magnesium, copper and zinc co-vary systematically across the 5xxx and 7xxx families that dominate the dataset, so part of the apparent dominance of magnesium may reflect this correlation structure rather than an independent physical effect. Gain-based importance is also a purely global attribution: it carries no information about the sign of a contribution, about how that contribution varies across the composition range, or about interactions between solutes. Permutation importance evaluated on held-out data would address the first concern, and SHAP attribution would address the second and third; neither was computed in the present work, and their absence is recorded among the limitations. The ranking should accordingly be read as a screening-level indication of which solutes dominate the resistivity response, corroborated independently by established scattering theory, rather than as a quantitative decomposition of that response.

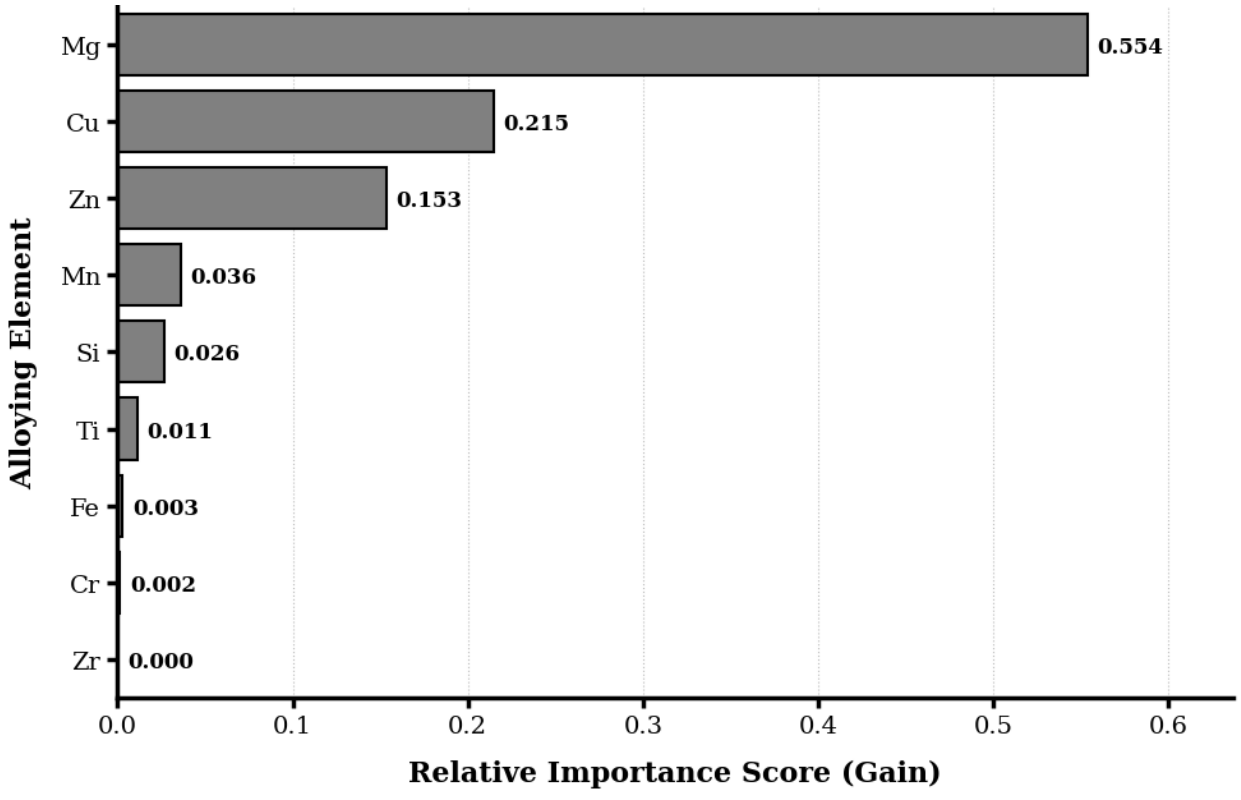

Figure 3 Relative importance of alloying elements in the XGBoost model for resistivity prediction.

Inverse design of high-resistivity aluminum alloys

After validating forward prediction accuracy, an inverse design step was applied to identify candidate aluminum alloy compositions with maximized electrical resistivity. In this screening process, the trained XGBoost model was used as a surrogate evaluator to rapidly predict

resistivity across a set of hypothetical compositions sampled within and slightly beyond the training bounds. The top 10 candidates are listed in Table 3.

A notable outcome is that the predicted resistivity values of the highest-ranked candidates fall within 9.26–9.52 μΩ·cm, substantially exceeding the maximum resistivity observed in the curated dataset (6.40 μΩ·cm). This gap indicates that the model has identified a region of the composition space that is underrepresented in the available data but is predicted to provide significantly enhanced resistive behavior. Such extrapolative predictions must be interpreted cautiously because both ensemble and kernel models can degrade outside their training domain; best practice therefore recommends validation using domain knowledge and the imposition of physical constraints derived from phase stability and solubility limits (Liang et al., 2022; Mafra Monfredo Ferreira et al., 2024). The compositional pattern across the top-ranked designs strongly corroborates the feature importance results. All proposed alloys exhibit high Mg (4.29–6.05 wt.%), Cu (6.46–7.56 wt.%), and Zn (7.84–9.29 wt.%) contents, consistent with the expectation that resistivity increases with solute-driven scattering intensity. The compositions resemble heavily alloyed Al–Zn–Mg–Cu systems (7xxx-series-like), suggesting that extreme solute loading is an effective strategy for maximizing resistivity within aluminum-based alloys. However, such high solute fractions may introduce manufacturability and phase-stability challenges (e.g., hot cracking susceptibility, brittle intermetallic formation), which motivates future CALPHAD-based screening and experimental verification as part of a constrained inverse-design pipeline (Zhang et al., 2026; Tao et al., 2026; Mafra Monfredo Ferreira et al., 2024).

Applicability domain and degree of extrapolation

Because the candidates in Table 3 are the output of a surrogate evaluated outside the region in which it was fitted, the degree of extrapolation was quantified explicitly rather than merely acknowledged. Considered one element at a time, the exceedance appears moderate. Copper ranges from 6.47 to 7.56 wt.% against a training maximum of 6.30 wt.% (up to +20%), zinc from 7.84 to 9.29 wt.% against 7.80 wt.% (up to +19%), zirconium from 0.176 to 0.204 wt.% against 0.175 wt.% (up to +17%), and magnesium reaches 6.05 wt.% against 5.10 wt.% (+19%). Copper, zinc and zirconium exceed the training maximum in all ten candidates; magnesium in five; iron and titanium in two each; silicon, manganese and chromium in none.

Considered jointly, however, the extrapolation is severe. The ten candidates carry between 24.2 and 32.3 wt.% total solute, leaving an aluminium balance of only 67.7 to 75.8 wt.%. For comparison, the most heavily alloyed commercial compositions represented in the training set are of the 7xxx type, whose total solute content is of the order of 10 wt.% with an aluminium balance above 88 wt.%. The candidate compositions therefore do not sit marginally outside

the training domain; they occupy a region of composition space in which the dataset contains no observations whatsoever, and in which the designation “aluminium alloy” is itself open to question. This is a direct consequence of applying the sampling bounds element by element: each individual constraint is satisfied while their conjunction is not. A tree-ensemble surrogate has no mechanism for signalling this condition, because it extrapolates by returning the value associated with the nearest terminal region of the fitted trees. That behaviour is visible in the results themselves. The ten candidates differ substantially from one another in composition, with silicon spanning 0.99 to 9.45 wt.% and magnesium 4.29 to 6.05 wt.%, yet their predicted resistivities cluster within 0.26 μΩ·cm of one another, at 9.26 to 9.52 μΩ·cm. The flatness of that band is a symptom of saturation at the boundary of the training data rather than evidence of a genuine plateau in the resistivity response, and it should be read as a diagnostic that the model has left its applicability domain. Accordingly, the entries in Table 3 are reported as an indication of the direction in which the model expects resistivity to increase, namely simultaneous loading of magnesium, copper and zinc, and not as alloy candidates. No claim of predictive accuracy is made for the numerical resistivity values, and no prediction interval is quoted for them, because a meaningful uncertainty estimate in this region would require either a probabilistic surrogate whose posterior variance grows away from the data, such as a Gaussian process, or a distribution-free conformal prediction wrapper calibrated on held-out residuals. Neither was implemented in the present work, and both are identified below as necessary components of a revised pipeline.

Table 3 Top 10 candidate aluminum alloy compositions designed for high electrical resistivity using the XGBoost inverse modeling framework.

Rank	Si (wt%)	Fe (wt%)	Cu (wt%)	Mn (wt%)	Mg (wt%)	Cr (wt%)	Zn (wt%)	Ti (wt%)	Zr (wt%)	Predicted Resistivity (μΩ·cm)
1	5.1325	0.4255	6.5225	0.9283	5.9306	0.0687	9.2419	0.1527	0.1847	9.5173
2	0.9897	1.0629	7.1419	1.1749	4.9422	0.0248	8.6765	0.0195	0.1758	9.5172
3	4.2691	0.9687	7.1837	0.9439	5.7023	0.0262	9.0971	0.0694	0.1941	9.4933
4	7.0324	0.5866	6.5987	0.9896	6.0509	0.1251	8.6245	0.1723	0.2032	9.4204
5	6.2874	0.5693	6.5169	0.8589	5.8709	0.0717	8.2489	0.1988	0.1959	9.4095
6	6.2972	0.8429	6.9026	1.0237	4.5501	0.1904	8.7096	0.2090	0.1787	9.3577
7	6.9303	0.8168	7.5600	1.1540	4.7116	0.1194	8.6171	0.0688	0.2041	9.3017
8	7.3856	0.6859	7.1177	1.0558	4.5613	0.2047	7.8446	0.0914	0.1793	9.2989
9	3.9261	0.7749	6.8837	1.0217	4.2916	0.2219	9.2903	0.0112	0.1978	9.2645
10	9.4487	1.0771	6.4649	0.8458	5.5252	0.2428	8.2672	0.2171	0.1864	9.2607

Discussion

The results obtained in this study indicate that the electrical resistivity of aluminium alloys is systematically predictable from composition alone, and that composition engineering guided by machine learning offers a plausible route towards addressing the long-standing limitation of aluminium as a microheater material. By increasing resistivity while retaining CMOS compatibility and low-temperature processability, the proposed approach bridges the gap between cost-effective manufacturing and energy-efficient resistive heating, which has traditionally been dominated by platinum or polysilicon-based solutions. From a microheater operation perspective, the observed increase in resistivity has direct implications for operating current and power requirements. For a fixed heater geometry, resistance scales linearly with material resistivity according to $R = \rho L/A$. Consequently, higher resistivity enables the same target temperature to be reached at a reduced current, as dictated by Joule heating relationships ($P = I^2R$). Lower operating currents would be expected to alleviate electrical stress on driving circuitry and to reduce electromigration risk, since electromigration flux scales with current density. It must be stressed that this is a scaling argument rather than a demonstrated result. No electrical, thermal or device-level measurement is reported in this work, and resistivity alone does not determine microheater performance, which depends additionally on the temperature coefficient of resistance, on thermal conductivity and heat loss to the substrate, on film adhesion, and on thermomechanical stability under repeated cycling. Higher resistivity also raises the drive voltage required to deliver a given power, which may itself constrain low-voltage battery operation, so the trade-off is not unidirectional. The efficiency implications set out here are therefore stated as expectations following from the Joule-heating relations, and they remain to be tested experimentally. The comparative modeling results further confirm that resistivity–composition relationships in multicomponent aluminum alloys are strongly non-linear. The pronounced performance gap between Linear Regression and non-linear models, particularly ensemble tree methods, reflects the underlying metallurgical complexity arising from interacting solute effects, lattice distortion, and microstructural pathways such as precipitation. XGBoost emerged as the most reliable surrogate model, combining high predictive accuracy with stable cross-validation performance. This finding aligns with broader trends in materials informatics, where gradient-boosting methods consistently outperform kernel-based and linear approaches when datasets exhibit compositional diversity and complex feature interactions. Interpretability analysis provides a physically meaningful link between machine learning outputs and metallurgical mechanisms. The dominance of magnesium, followed by copper and zinc, in the feature importance ranking corroborates established theories of solid-solution electron scattering and impurity-driven resistivity enhancement in aluminum alloys. High Mg content

induces significant lattice distortion, increasing electron scattering, while Cu and Zn introduce additional scattering centers and promote precipitate or intermetallic formation that further modifies electron transport. The negligible influence of Fe, Cr, and Zr within the studied ranges suggests that trace elements contribute marginally compared to major solutes, reinforcing the conclusion that resistivity optimization in aluminum alloys is primarily governed by high-impact solute additions rather than micro-alloying. The inverse design results extend the accessible resistivity space beyond the bounds of the experimental dataset, identifying candidate compositions with predicted resistivity values of 9.26–9.52 μΩ·cm. These compositions consistently resemble heavily alloyed Al–Zn–Mg–Cu systems, analogous to 7xxx-series alloys, indicating that extreme solute loading is an effective strategy for maximizing resistivity. From an application standpoint, such resistivity levels could enable substantial reductions in operating current for microheaters, improving power efficiency and relaxing constraints on peripheral electronics. However, these benefits must be weighed against potential trade-offs inherent to high-solute aluminum alloys. Increasing solute concentrations in Al–Zn–Mg–Cu systems introduces several manufacturability and reliability challenges. Elevated alloying levels can reduce castability, narrow processing windows, and increase susceptibility to hot cracking during solidification. High Zn and Cu contents may also exacerbate corrosion sensitivity and promote the formation of brittle secondary phases, while excessive solid-solution strengthening can compromise ductility. These trade-offs underscore that resistivity maximization alone is insufficient for practical deployment; instead, alloy design must balance electrical performance with phase stability, mechanical robustness, and process compatibility.

From bulk-alloy data to thin-film microheaters

A further limitation conditions every application-level statement in this work: the model is trained on bulk-alloy resistivity measured at 20 °C, whereas the intended application is a sputtered or evaporated film a few hundred nanometres thick. The two quantities are not interchangeable. When film thickness approaches the electron mean free path in aluminium, which is of the order of 15 to 20 nm at room temperature, grain-boundary scattering and diffuse surface scattering contribute resistivity terms that are absent from a bulk measurement and that scale inversely with thickness and with grain size, as described by the Mayadas–Shatzkes and Fuchs–Sondheimer treatments. Measured thin-film resistivities in aluminium commonly exceed the bulk value by a factor of the order of two, and that factor is set by deposition conditions rather than by composition. Deposition therefore acts as an independent variable that the present feature space does not represent. Substrate temperature, deposition rate and working pressure determine the as-deposited grain size, while subsequent annealing coarsens the grains and simultaneously redistributes solute

through precipitation, so that two films of identical composition can differ substantially in resistivity. In a heavily supersaturated Al–Zn–Mg–Cu film the situation is more acute, because thermal cycling during microheater operation would itself drive precipitation: resistivity would then drift with operating history rather than remaining a fixed material constant, which is precisely the failure mode that disqualifies a heater material irrespective of its initial resistivity. Native and thermally grown oxide reduces the effective conducting cross-section and shifts measured sheet resistance, and the rapid quench inherent to physical vapour deposition may retain solute well beyond equilibrium solubility, which raises resistivity but at the cost of thermal stability.

The practical consequence is that the bulk resistivity predicted here should be treated as a lower bound and as a compositional ranking signal, not as the resistivity a fabricated film would exhibit. Extending the framework to thin films would require either a dataset of measured thin-film resistivities with deposition metadata, or an explicit physical correction layer in which the predicted bulk value is combined with a Mayadas–Shatzkes term parameterised by measured grain size and thickness. Neither is attempted here, and direct thin-film measurement on any shortlisted composition is a prerequisite for any device-level claim. In this context, the present results should be interpreted as a first-stage screening rather than a finalized alloy solution. Best practice in materials informatics increasingly advocates for hybrid inverse-design pipelines that integrate machine learning with physics- and thermodynamics-based constraints. Incorporating CALPHAD-informed bounds, phase fraction limits, and solubility constraints would enable the exclusion of compositions prone to undesirable phase formation or brittle behavior, thereby improving trustworthiness and manufacturability of ML-designed alloys. Such constrained optimization frameworks can substantially reduce the risk of extrapolative failure while preserving the efficiency gains of data-driven screening. Validation of the proposed high-resistivity alloys remains a critical next step. Experimental synthesis followed by direct resistivity measurements would provide definitive confirmation of model predictions. Thin-film deposition studies are particularly relevant for microheater applications, as they replicate realistic geometries and thermal environments. Ultimately, fabrication and testing of functional microheater prototypes would allow comprehensive evaluation of electrical performance, thermal stability, and reliability under cyclic operation. These validation pathways are essential to translate computational predictions into deployable technologies. The corresponding experimental route can be specified concretely. Shortlisted compositions would be prepared from high-purity elemental stock by induction or arc melting under an inert atmosphere, homogenised, and sectioned into specimens of defined geometry. Bulk electrical resistivity would be measured by the four-probe method at 20 °C in accordance with ASTM B193, with at least three specimens per

composition to establish reproducibility, and the measured values compared directly against the model prediction so that an out-of-domain error estimate is obtained rather than assumed. In parallel, thin films would be deposited by magnetron sputtering from alloy targets of matched composition onto thermally oxidised silicon, patterned into van der Pauw and four-point structures by standard photolithography, and characterised for sheet resistance, for temperature coefficient of resistance across the intended operating window, and for resistance drift under repeated thermal cycling. Film thickness, grain size and phase content would be recorded by profilometry, electron microscopy and X-ray diffraction, so that any difference between bulk and thin-film resistivity can be attributed to specific scattering contributions rather than absorbed into an empirical correction factor. Only at that point would fabrication of a functional microheater and measurement of its power-to-temperature characteristic constitute a meaningful test of the energy-efficiency argument advanced above.

Concretely, the constrained pipeline now under development operates in the following order. Compositions generated by the sampler are first filtered by a hard aluminium-balance constraint, for example a requirement that aluminium constitute at least 88 wt.% of the alloy; this single screen already excludes all ten candidates listed in Table 3. Surviving compositions are then evaluated against a commercial aluminium thermodynamic database, and are rejected if the equilibrium volume fraction of brittle intermetallic phases at the intended solution-treatment temperature exceeds a defined threshold, or if the solidification interval obtained from a Scheil–Gulliver calculation exceeds the range associated with hot-tearing susceptibility in Al–Zn–Mg–Cu systems (Zhang et al., 2026). Only compositions passing both screens are ranked by predicted resistivity, and the ranking is reported together with a conformal prediction interval so that predictions resting on extrapolation are visibly distinguished from those supported by data. This ordering, in which the physical constraints are applied before rather than after the surrogate prediction, is the substantive difference between the screening exercise reported here and a deployable design tool. From a broader perspective, this work demonstrates how explainable machine learning can transform alloy development from an empirical, trial-and-error process into a predictive, data-guided workflow. By coupling surrogate modeling with physically interpretable insights, the proposed framework enables rational navigation of high-dimensional composition spaces while maintaining alignment with metallurgical principles. The methodology is not limited to resistivity optimization or aluminum alloys; rather, it provides a generalizable blueprint for designing functional materials tailored to microscale devices. Overall, the integration of materials science knowledge with machine learning-based inverse design offers a credible and scalable pathway toward CMOS-compatible, low-cost, and energy-efficient microheater materials. While further validation and constraint integration are required, the present study

establishes a strong foundation for data-driven resistive material design and highlights the potential of aluminum alloys as viable alternatives to conventional microheater materials when their properties are engineered rather than substituted.

Conclusions

This study addressed the intrinsic limitation of aluminium as a microheater material its low electrical resistivity by treating resistivity as a designable property rather than a fixed constraint, and by using machine learning to navigate the compositional space efficiently. Four supervised regression models were benchmarked on a curated dataset of 220 commercial aluminium alloys described solely by composition. Extreme Gradient Boosting delivered the highest accuracy (R^2 = 0.861; MAPE = 3.9%) and retained stable performance under K-fold cross-validation (CV-R^2 = 0.839; CV-RMSE = 0.396 μΩ·cm), while the linear baseline performed substantially worse (R^2 = 0.635). This gap provides quantitative evidence that resistivity in multicomponent aluminium alloys arises from interacting solute effects that cannot be captured by linear superposition. Feature importance analysis attributed approximately 92% of the model's explanatory power to magnesium (0.554), copper (0.215), and zinc (0.153), with Fe, Cr, and Zr contributing negligibly within the concentration ranges sampled. This ranking is consistent with established solid-solution and impurity scattering mechanisms, indicating that the model captured metallurgically meaningful relationships rather than dataset artefacts. Surrogate-based inverse screening identified heavily alloyed Al–Zn–Mg–Cu compositions with predicted resistivity of 9.26–9.52 μΩ·cm. These values exceed the maximum observed in the training data (6.40 μΩ·cm), and the corresponding solute loadings exceed conventional solubility limits in aluminium. The candidates should therefore be interpreted as an extrapolative indication of a promising direction in composition space, not as deployable alloy specifications. Three steps are required to convert these predictions into practical materials. First, thermodynamic screening, for example CALPHAD-based phase-stability and solubility constraints should be integrated into the inverse design loop to exclude compositions prone to brittle intermetallic formation or hot tearing. Second, the shortlisted compositions require experimental synthesis and direct four-point resistivity measurement. Third, thin-film deposition and microheater prototyping are needed to confirm that bulk resistivity gains translate into reduced operating current, since thin-film resistivity is additionally governed by grain-boundary and surface scattering not represented in this dataset. More broadly, this work demonstrates that a composition-only machine learning framework, coupled with interpretability analysis, can convert alloy development for functional microscale devices from a trial-and-error exercise into a directed search. The approach generalises beyond resistivity and beyond aluminium to other property-targeted alloy design problems.

Limitations

The limitations of this study are stated explicitly. First, the feature space is compositional only: processing route, temper designation, grain size and heat-treatment history are not represented, although each materially affects resistivity. This places a ceiling on achievable accuracy that is not attributable to the choice of algorithm, and it means that two alloys of identical nominal composition, but different temper appear to the model as a single point with two different labels. Second, the dataset comprises 220 records drawn from a single public source, and its coverage of composition space is neither uniform nor independent, since commercial alloys cluster into families; performance estimates obtained by random splitting are consequently optimistic relative to those that grouped splitting across alloy families would yield. Third, where the source specifies composition as a permitted range, a single representative value was substituted, introducing label noise of known sign but unquantified magnitude. Fourth, model selection and cross-validated reporting share the same folds, so the cross-validated statistics carry a mild optimistic bias; the hold-out metrics do not. Fifth, interpretability rests on gain-based importance alone, without permutation importance or SHAP attribution. Sixth, the inverse-design step is unconstrained, its output lies outside the multivariate training domain, and no uncertainty quantification is attached to it. Seventh, all measurements underlying the training data are bulk measurements at a single temperature, whereas the target application is a thin film operating across a temperature range. The fourth, fifth and sixth of these are the subject of ongoing work, in which nested cross-validation, SHAP attribution, conformal prediction intervals and CALPHAD-based phase-stability screening are being integrated into a single constrained pipeline.

Data Availability

The curated dataset of 220 aluminium alloy compositions and their corresponding electrical resistivity values, together with the alloy designations, the analysis scripts, the selected hyperparameters and the random seeds required to reproduce every result reported in this manuscript are additionally available from the corresponding author on request. The analysis was carried out in Python using scikit-learn and xgboost

Declaration of Generative AI

During the preparation of this work, the authors used Trinka AI in order to improve the language, grammar, and readability of the manuscript. After using this tool, the authors reviewed and edited the content as needed and take full responsibility for the content of the publication.

References

Abdo, H. S., Seikh, A. H., Mohammed, J. A., & Soliman, M. S. (2021). Alloying elements effects on electrical conductivity and mechanical properties of newly fabricated Al based alloys produced by conventional casting process. Materials, 14(14), 3971. https://doi.org/10.3390/ma14143971

Alshwawreh, N., Alhamarneh, B., Altwarah, Q., Quandour, S., Barghout, S., & Ayasrah, O. (2021). Electrical resistivity and tensile strength relationship in heat-treated all aluminum alloy wire conductors. Materials, 14(19), 5738. https://doi.org/10.3390/ma 14195738

Bai, J., Gao, M., Wang, C., Pei, J., Yang, L., & Guan, R. (2025). Role of Er element and two-stage heat treatment in a rheo-extruded Al–Sc–Zr alloy: Balance strength and electrical conductivity. Materials & Design. https://doi.org/10.1016/j.matdes. 2025. 115096

Cui, X., Ye, H., Liu, H., Li, X., Man, Q., Li, H., Cui, H., Feng, R., & Pan, Y. (2023). The improvement mechanism of good matching between electrical conductivity and mechanical properties for Al-4Si-0.8Mg-0.6Fe alloy. Journal of Alloys and Compounds. https://doi.org/10.1016/j.jallcom.2022.168275

Elamin, N. Y., Elamin, M. R., Salih, M., Younis, M. K., Fathy, A., Ibrahim, N. M. A., & Habba, M. I. A. (2025). Machine learning-enabled discrete transfer function modeling and optimization of mechanical properties in ARB-fabricated Al/Ni/SiC nanocomposites. Materials Today Communications. https://doi.org/10.1016/j.mtcomm.2025.113777

Genc, M., Eloi, P., Blandin, J.-J., Pascal, C., Donnadieu, P., De Geuser, F., Lhuissier, P., Desrayaud, C., & Martin, G. (2022). Optimization of the strength vs. conductivity trade-off in an aluminium alloy designed for laser powder bed fusion. Materials Science and Engineering: A. https://doi.org/10.1016/j.msea.2022.144139

Jeroish, Z. E., Bhuvaneshwari, K. S., Samsuri, F., & Narayanamurthy, V. (2022). Microheater: Material, design, fabrication, temperature control, and applications—A role in COVID-19. Biomedical Microdevices, 24(1), 3. https://doi.org/10.1007/s10544-021-00595-8

Kalinin, I. A., Roslyakov, I. V., Khmelenin, D. N., & Napolskii, K. S. (2023). Long-term operational stability of Ta/Pt thin-film microheaters: Impact of the Ta adhesion layer. Nanomaterials, 13(1), 94. https://doi.org/10.3390/nano13010094

Khan, M. S., & Sasikumar, C. (2025). Tracking microstructural evolution and hardening in Al–Zn–Mg–Cu alloys aged artificially via electrical conductivity measurements. Proceedings of the Institution of Mechanical Engineers, Part L: Journal of Materials: Design and Applications. https://doi.org/10.1177/14644207241264373

Krishna, R. M., Eftekhar, A., Lee, S., Fan, T., Wu, X., Hosseinnia, A., Wang, H., Swaminathan, M., & Adibi, A. (2022). Polysilicon micro-heaters for resonance tuning in CMOS photonics. Optics Letters, 47(5), 1097–1100. https://doi.org/10.1364/OL.441510

Kwak, S., Kim, J., Ding, H., Xu, X., Chen, R., Guo, J., & Fu, H. (2022). Machine learning prediction of the mechanical properties of γ-TiAl alloys produced using random forest regression model. Journal of Materials Research and Technology. https://doi.org/10.1016/j.jmrt.2022.02.108

Li, D., Ruan, Y., Chen, C., He, W., Chi, C., & Lin, Q. (2022). Design and thermal analysis of flexible microheaters. Micromachines, 13(7), 1037. https://doi.org/10.3390/mi13071037

Liang, T., Wang, J., Xue, C., Zhang, C., & Zhang, M. (2022). Design of high strength and electrically conductive aluminium alloys by machine learning. Materials Science and Technology, 38(2), 116–129. https://doi.org/10.1080/02670836.2022.2025560

Liu, M., Shan, Z., Li, X., Zang, Y., & Yan, D. (2025). Research on the effect of solution treatment on mechanical properties, electrical conductivity and microstructure of cold-rolled 7075 aluminum alloy. Materials Letters. https://doi.org/10.1016/j.matlet.2025.138532

Mafra Monfredo Ferreira, V. H., Coury, F. G., de Araujo Santana, D., & Koga, G. Y. (2024). Novel high nitrogen austenitic stainless steels: From high-throughput screening to experimental validation and properties relationship. Journal of Materials Research and Technology. https://doi.org/10.1016/j.jmrt.2024.03.090

Padhy, S. P., Davidson, K. P., Tan, L. P., Varma, V. B., Sharma, V. K., Tan, X., Wei, Y., Xu, X., Hippalgaonkar, K., Jhon, M. H., & Ramanujan, R. V. (2025). Integrated design framework for titanium aluminides through interpretable machine learning. Journal of Alloys and Compounds. https://doi.org/10.1016/j.jallcom.2025.184937

Tao, S., Yu, M., Li, Y., Wen, K., Li, X., Li, Z., Zhang, Y., & Xiong, B. (2026). Study on the influence of precipitation characteristics on fatigue properties of typical 7xxx aluminum alloys. Materials, 19(8), 1601. https://doi.org/10.3390/ma19081601

Yavari, F., Javidani, M., Pan, L. R., & Chen, X.-G. (2025). Synergistic effects of cerium and magnesium on optimizing electrical conductivity and mechanical properties of AlSi3 cast alloys. Advanced Engineering Materials. https://doi.org/10.1002/adem.202402647

Zhang, H., Rong, L., Ma, C., Wei, W., Huang, H., Zhang, D., Wen, S., Gao, K., & Wu, X. (2026). Er and Zr microalloying and hot tearing susceptibility of Al-30Zn-2Cu high-zinc aluminum alloys. International Journal of Metalcasting. https://doi.org/10.1007/s40962-025-01619-2